Molecular Structure Corporation (1989). *TEXSAN. Single-Crystal Structure Analysis Software.* Version 5. Molecular Structure Corporation, 3200A Research Forest Drive, The Woodlands, TX 77381, USA.
OKAYA, Y. (1969). *Acta Cryst.* B**25**, 1882–1889.
OTTERSEN, T., ROMMING, C. & SNYDER, J. P. (1976). *Acta Chem. Scand. Ser. B*, **30**, 407–416.
SCHAEFER, J. P. & WALTHERS, K. K. (1971). *Tetrahedron*, **27**, 5281–5287.
WATSON, W. H., KASHYAP, R. P., MARCHAND, A. P. & VIDYASAGAR, V. (1989). *Acta Cryst.* C**45**, 2010–2012.
ZACHARIASEN, W. H. (1968). *Acta Cryst.* A**24**, 212–216.
ZHANG, D. (1985). *SVDHA.* Program to calculate molecular volume, area and accessible surface area. Unpublished.

Acta Cryst. (1992). B**48**, 837–848

Charge Density Studies on Small Organic Molecules Around 20 K: Oxalic Acid Dihydrate at 15 K and Acetamide at 23 K

BY DIETER ZOBEL, PETER LUGER AND WOLFGANG DREISSIG

Institut für Kristallographie, Freie Universität Berlin, Takustrasse 6, *D*-1000 *Berlin* 33, *Germany*

AND TIBOR KORITSANSZKY

Central Research Institute for Chemistry of the Hungarian Academy of Sciences, H-5025 *Budapest, Hungary*

(*Received* 9 *December* 1991; *accepted* 15 *May* 1992)

Abstract

High-resolution X-ray diffraction data were collected for oxalic acid dihydrate at 15 K and for acetamide at 23 K (and at 100 K for comparison) to obtain accurate crystal data and experimental electron density. The measurements were performed with a large full-circle Eulerian cradle (400 mm diameter) with an offset χ circle equipped with a double-stage He refrigerator (Displex DE 202) and a Be vacuum chamber around the cold head. Conventional and multipole refinements were carried out on the data. Deformation density maps were generated by $X-X$ Fourier syntheses and compared with the static distribution obtained from the multipole model. Results are also compared with those reported previously. The change in the resolution of the deformation density due to the improved accuracy of the high-order data is analyzed. For the acetamide molecule the temperature dependence of the measured intensities and the thermal parameters are also examined.

Introduction

In order to obtain accurate molecular data and static electronic properties from X-ray diffraction observations the vibrational smearing of the electron density due to atomic motion should be properly decomposed from the asphericity due to chemical bonds. In any scattering formalism applicable for this task the parameters accounting for the two effects are expected to be strongly correlated. Reflections detected at low scattering angles carry information about the diffuse characteristics of the electron density, while high-order data are mainly affected by the sharp features of the distribution near to the nucleus. The number of observable intensity data for a given crystal and experimental conditions is limited. One way to increase the resolution of the diffraction data at high scattering angles is to decrease the temperature and so the delocalization of the electron density caused by vibrational smearing. This is why the experiment should be carried out at the lowest temperature feasible for a single-crystal diffractometer.

For neutron scattering, temperatures of around 20 K have been realized for more than ten years (Allibon, Filhol, Lehmann, Mason & Simms, 1981) and a number of neutron structure determinations at this very low temperature have been reported (Jeffrey, Ruble, McMullan, De Frees, Binkley & Pople, 1980; Jeffrey, Ruble & Yates, 1983, and papers cited therein; Weber, Craven, Sawzik & McMullan, 1991). Although cryostats for this temperature have also been mounted on X-ray diffractometers in a few cases (Hendriksen, Larsen & Rasmussen, 1986), most single-crystal X-ray data sets are still collected around 100 K using conventional nitrogen gas stream devices. The advantages of neutron data at 20 K cannot be utilized unless the corresponding X-ray data are available. One of the few exceptions is reported by Coppens & Lehmann (1976), who carried out a charge-density study at 30 K using a liquid-helium cooling device.

Based on our earlier experiences with a single-stage cryostat at 50 K (Zobel & Luger, 1990) we

0108-7681/92/060837-12$06.00

established a 20 K double-stage system for X-ray diffraction experiments that should permit measurement of high-resolution X-ray data sets to be used in charge-density determinations at this temperature.

For the initial investigation oxalic acid dihydrate was chosen for redetermination. This compound is one of the best documented examples, and so a comparison could easily be made. It was investigated in the course of an IUCr project in several laboratories in the early eighties (later reported by Coppens, 1984), so that it can be regarded as a kind of 'standard' in the field of electron deformation density. The second compound investigated was acetamide whose structure has also been examined several times (Hamilton, 1965; Denne & Small, 1971; Ottersen, 1975). In addition, the charge density has been studied at 80 K (Ottersen, Alnlöf & Hope, 1980), and moreover, accurate neutron data at 23 K are available (Jeffrey *et al.*, 1980). Hence, it seemed possible to combine X-ray and neutron data to give an electron deformation density map at 23 K which has not yet been reported at such a low temperature. Detailed *ab initio* molecular orbital studies were also described by Jeffrey *et al.* (1980).

Experimental set-up

Encouraged by the experiments and some promising results from our 50 K single-stage cooling system (Zobel & Luger, 1990) we mounted a double-stage closed-cycle refrigerator (Displex, Air Products, USA) on a large Eulerian cradle with an offset χ circle of 400 mm diameter (Huber, type 512). The vacuum chamber was made of stainless steel with a cylindrical window of Be (5 mm wall thickness) for minimum X-ray absorption. The Displex was mounted, together with the cryostat, on an X–Y–Z cylindrical dove-tail movement in order to allow crystal alignment. Vacuum (less than 1×10^{-4} mbar) was achieved with a turbomolecular pump which was then disengaged during data collection. The cryopump activity of the first stage of the refrigerator provides a good vacuum, so that the temperature could be held constant at around 20 ± 0.5 K for a long period of time, in one case for up to 30 days.

The crystal was mounted on a tapered holder (OFHC copper) very similar to that described in our previous paper (Zobel & Luger, 1990) and screwed onto the cold head of the second stage.

Crystal alignment was first controlled optically, and later, when the specimen was hidden from view inside the Be cryostat, by X-ray diffraction *via* the 'C8 routine'. In this case a reflection was centered at its eight equivalent positions (King & Finger, 1979).

The temperature was measured with an Au(Fe)/chromel thermocouple fixed in a small hole at the tip of the second stage and was calibrated *via* an Si diode, fixed close to it. Temperature stability was better than 0.5 K, and the absolute reading less than 2 K after thermal compensation.

The diffractometer used was a complete four-circle set up (Huber, type 5042) equipped with additional limit switches to avoid damage to the He hoses. It was controlled by an inhouse-designed single-board interface computer using an MC68008 processor. The program for the interface was written in the 'Pearl' language on an Atari 1040ST and loaded into the EPROM memory of the board. The use of an Atari computer seemed to be quite convenient at low budget, and very powerful in practical work (Lange, Burzlaff & Neugebauer, 1988). A more detailed description of the diffractometer arrangement including motor driver, interface, extension of the D4 crystallographic software, reflection-profile correction, MicroVAX communication as well as the temperature-controlled cooling process will be published elsewhere.

For all experiments Nb-filtered Mo $K\alpha$ radiation was used at 50 KV and 40 mA (stabilized HF generator: Seifert, ISO-Debyeflex 3000). To test the mechanical stability of the Eulerian cradle under the load of the Displex (6.8 kg) we used a spherical ruby crystal (courtesy of Dr J. Gabe, National Research Council, Ottawa, Canada) of 0.152 (5) mm diameter with hexagonal lattice constants reported to be $a =$ 4.76099 (6) and $c = 12.99625$ (35) Å. By means of the C8 routine we determined crystal alignments, half-shutter position and zero settings of the diffractometer circles. From the centering of 71 reflections ($30 \le 2\theta \le 80°$) the ruby lattice parameters were determined as $a = 4.7617$ (4) and $c = 13.0013$ (10) Å which is within 2σ for a and 5σ for c in accordance with the exceptionally precise data given by Gabe (1981), confirming the proper alignment of this rugged instrument.

Oxalic acid dihydrate

Measurements

A prismatic crystal $0.3 \times 0.2 \times 0.5$ mm was fixed with special araldite glue on the mounting described in our previous paper (Zobel & Luger, 1990) and sealed in a capillary (0.01 mm wall thickness). To check the crystal quality, a room-temperature data set was collected in the range $5 \le 2\theta \le 50°$. Conventional refinement (*XTAL*2.2; Hall & Stewart, 1987) with starting parameters from Stevens & Coppens (1980) converged to an R value of 0.028 ($wR = 0.030$) and proved the crystal to be suitable for further measurements. The crystal was then cooled down slowly to 15 ± 3 K in steps of 2 K within a total time of about 4 h. The lattice parameters and crystal orientation were determined by centering 54 reflec-

tions every 50 K. For several reflections φ scans were monitored in order to control the crystal quality. Splitting of the reflection-profile maximum due to thermal tension was observed only once.

During preliminary work and data collection over six days the temperature could be kept constant to within ± 0.5 K. The setting angles of 86 reflections were used in a least-squares calculation to determine the final crystal orientation and cell parameters. Two complete data sets each within a half sphere in the range $5 \le 2\theta \le 104°$ were measured ($-27 \le h \le 30$, $-30 \le k \le 24$, $-24 \le l \le 27$) resulting in 7369 reflections, so that four observations per independent general reflection were present. Since the relative increase in intensity is remarkable at 20 K compared to 100 K, particularly for high-order reflections (see acetamide below), only 8.0% of the reflection intensities were below 2σ. The overall agreement between symmetry-equivalent reflections, using all data, was $R_{int} = 0.018$ (program *SORTRF* in *XTAL*2.2). An absorption correction was applied (*ABSORB* in *XTAL*2.2) so as to obtain reliable path lengths for the extinction correction, whereas the absorption itself has practically no influence because $\mu d = 0.08$ and the max./min. absorption factor = 1.002/1.001. Crystallographic data and refinement results are summarized in Table 1 and compared with room-temperature data.

Table 1. *Crystallographic and least-squares refinement data for oxalic acid dihydrate at* 15 K *in comparison to room-temperature results*

Space group: $P2_1/n$, $Z = 2$, $F(000) = 132$, $M_r = 128.08$, λ(Mo $K\alpha$) = 0.71069 Å (Nb filtered).

	Room temperature	15 K	
a (Å)	6.115 (2)	6.093 (2)	
b (Å)	3.601 (1)	3.469 (1)	
c (Å)	12.050 (3)	11.926 (2)	
β (°)	106.31 (2)	105.69 (2)	
V (Å^3)	256.21	242.64	
D_x (g cm^{-3})	1.637	1.726	
μ (cm^{-1})	1.86	1.96	
		Full order	High order
2θ (°)	5–50	5–104	60–104
$\sin\theta/\lambda$ (Å^{-1})	0.08–0.64	0.08–1.08	0.71–1.08
$N_{measured}$	1443	7369	
N_{unique}	555	1822	1223
Unobserved [$F_o < 2\sigma(F_o)$]	43	122	98
NV	51	51	38
R_{int} (%)	0.99	1.78	
R (%)	2.92	2.71	2.31
wR (%)	3.45	3.23	2.18
Goodness of fit	3.81	2.91	1.38
Multipole refinement			
N_{ref}		1725 [$F_o > 4\sigma(F_o)$]	
NV		115	
R (%)		1.41	
wR (%)		1.31	
Goodness of fit		1.210	

Structure refinement

(*a*) *Conventional refinement.* The 100 K data of Stevens & Coppens (1980) were taken as initial parameters. The quantity $\sum w(F_o - k|F_c|)^2$ with $w = 1/\sigma^2(F_o)$ was minimized using a full-matrix least-squares program (*SFLSX* link of *XTAL*2.2). In addition to the standard atomic parameters an isotropic extinction factor was included (maximum extinction correction: 0.96 for the 110 reflection). Several refinements were carried out choosing high-order cut-off's between 0.5 and 0.81 Å^{-1} in $\sin\theta/\lambda$. We found that increasing the cut-off value beyond 0.71 Å did not change the parameters significantly. The coordinates and isotropic displacement parameters of the H atoms were obtained from refinement of the full data set. A summary of the different refinements is given in Table 1. The positional parameters and geometrical data are listed in Tables 2 and 3, respectively.

It can be stated that the displacement parameters have only about half the values compared to 100 K (Stevens & Coppens, 1980) for both the case of full refinement and high-order refinement, except for H(1), for which the value of $U = 0.070$ (6) Å^2 seems quite high.

(*b*) *Multipole refinement.* Multipole refinement (*MOLLY*) was carried out on the basis of the spherical harmonics expansion of the valence density described by Hansen & Coppens (1978). The local coordinate system, the atomic site symmetries, core and valence scattering factors and the parameters of the Slater-type radial functions were chosen as for the 100 K study (Stevens & Coppens, 1980) so as to make the results directly comparable. An isotropic extinction parameter of type I with a Lorentzian mosaic distribution (Becker & Coppens, 1974) was included in the refinement. The H atoms were treated in the same way as in the above-mentioned study. Positional parameters were fixed at the values obtained by neutron diffraction at 100 K (Feld & Lehmann, 1979). Thermal parameters were estimated by scaling the neutron values by the average ratio of the X-ray (15 K) to neutron (100 K) parameters for the non-H atoms.

The atomic charges obtained (Table 4) are in good agreement with those of the 100 K study. Discrepancies in geometrical data (Table 3) and thermal parameters (Table 2) are smaller than 3σ as compared with the conventional high-order result.

Experimental deformation density

Electron deformation densities were calculated by $X - X$ difference Fourier syntheses. In Fig. 1 an $X_{low} - X_{high}$ map is shown in the plane of the molecule.

Calculated structure factors for spherical atoms were generated from the parameters of the high-order refinement. A cut-off limit of 0.71 Å^{-1} in $\sin\theta/\lambda$ was used in the summation.

Table 2. *Atomic parameters and displacement factors for oxalic acid dihydrate at* 15 K, *with e.s.d.'s in parentheses*

FO = full-order data: $0.07 \le \sin\theta/\lambda \le 1.078$ Å^{-1}, HO = high-order data: $0.71 \le \sin\theta/\lambda \le 1.078$ Å^{-1}, ML = results of multipole refinement. Displacement factors of the form $T(\text{aniso}) = \exp\{-2\pi^2[U_{11}(ha^*)^2 + U_{22}(kb^*)^2 + U_{33}(lc^*)^2 + 2U_{12}hka^*b^* + 2U_{13}hla^*c^* + 2U_{23}klb^*c^*]\}$, $T(\text{iso}) = \exp[-2U(2\pi\sin\theta/\lambda)^2]$, with U_{ij} and U in Å^2 × 100.

		x	y	z	U_{11}/U	U_{22}	U_{33}	U_{12}	U_{13}	U_{23}
C(1)	FO	−0.04488 (4)	0.05960 (8)	0.05206 (2)	0.58 (1)	0.69 (1)	0.52 (1)	0.059 (5)	0.166 (5)	−0.001 (5)
	HO	−0.04483 (3)	0.05952 (8)	0.05208 (2)	0.49 (2)	0.60 (2)	0.43 (2)	0.066 (5)	0.143 (5)	−0.001 (5)
	ML	−0.04481 (3)	0.05952 (5)	0.05208 (2)	0.496 (5)	0.655 (3)	0.43 (1)	0.098 (5)	0.139 (5)	0.016 (4)
O(1)	FO	0.08535 (3)	−0.05538 (8)	0.15036 (2)	0.76 (1)	1.08 (1)	0.46 (1)	0.235 (5)	0.125 (5)	0.051 (5)
	HO	0.08528 (3)	−0.05538 (8)	0.15036 (2)	0.67 (2)	0.99 (2)	0.38 (2)	0.232 (4)	0.102 (5)	0.050 (4)
	ML	0.08541 (3)	−0.05536 (5)	0.15036 (2)	0.673 (5)	1.011 (3)	0.400 (7)	0.232 (5)	0.104 (5)	0.048 (4)
O(2)	FO	−0.22152 (3)	0.24500 (7)	0.03631 (2)	0.67 (1)	1.00 (1)	0.67 (1)	0.283 (5)	0.206 (5)	0.030 (5)
	HO	−0.22149 (3)	0.24498 (7)	0.03632 (2)	0.58 (2)	0.91 (2)	0.58 (2)	0.290 (5)	0.180 (5)	0.031 (4)
	ML	−0.22157 (3)	0.24504 (5)	0.03630 (2)	0.587 (5)	0.945 (3)	0.58 (1)	0.288 (5)	0.178 (4)	0.035 (4)
O(3)	FO	−0.45156 (3)	0.63486 (8)	0.17848 (2)	0.80 (1)	1.08 (1)	0.62 (1)	0.148 (5)	0.248 (5)	0.073 (5)
	HO	−0.45161 (3)	0.63477 (7)	0.17846 (2)	0.72 (2)	0.99 (2)	0.54 (2)	0.146 (4)	0.227 (5)	0.074 (4)
	ML	−0.45152 (2)	0.63481 (6)	0.17851 (2)	0.720 (4)	1.020 (3)	0.55 (1)	0.127 (5)	0.232 (4)	0.072 (5)
H(1)	FO†	0.029 (3)	0.008 (6)	0.214 (2)	7.0 (6)					
	ML	0.02339	0.92171	0.02228	1.35	1.754	1.095	0.183	0.317	0.005
H(2)	FO†	−0.558 (2)	0.691 (4)	0.119 (1)	2.8 (3)					
	ML	−0.57832	0.69677	0.11269	1.430	2.245	1.250	0.400	0.010	0.320
H(3)	FO†	−0.364 (2)	0.470 (4)	0.150 (1)	3.6 (4)					
	ML	−0.35811	0.45457	0.14954	1.630	2.130	1.865	0.621	0.780	−0.150

† HO: same values as FO.

Table 3. *Bond lengths* (Å), *angles* (°) *and hydrogen bonds* (Å) *for oxalic acid dihydrate at* 15 K, *with e.s.d.'s in parentheses*

	Full order	High order
C(1)—O(1)	1.2884 (4)	1.2877 (4)
C(1)—O(2)	1.2239 (4)	1.2240 (4)
C(1)—C(1)	1.5423 (5)	1.5424 (4)
O(1)—H(1)	0.97 (2)	
O(3)—H(2)	0.85 (1)	(the same)
O(3)—H(3)	0.91 (2)	
O(1)—C(1)—O(2)	127.00 (3)	127.00 (2)
O(1)—C(1)—C(1)	112.60 (3)	112.70 (3)
O(2)—C(1)—C(1)	120.40 (2)	120.30 (2)
C(1)—O(2)—H(1)	113 (1)	(the same)
H(2)—O(3)—H(3)	103 (1)	

	Full order		High order	
	X—H···Y	H—X	H···Y	X—H···Y
O(1)—H(1)···O(3)	2.4832 (6)	0.97 (2)	1.52 (2)	2.4830 (6)
O(2)—H(2)···O(3)	2.8182 (6)	0.85 (1)	1.98 (1)	2.8182 (6)
O(2)—H(3)···O(3)	2.8182 (6)	0.91 (2)	1.96 (2)	
O(2)—H(2)···O(3)	2.8201 (6)	0.85 (1)	1.98 (1)	2.8201 (6)
O(2)—H(3)···O(3)	2.8201 (6)	0.91 (2)	1.96 (2)	

Table 4. *Multipole refinement population parameters for oxalic acid dihyrate at* 15 K

E.s.d.'s of P_{lm} (l,m = 0) are less than 0.02, and for P_{lm} ($l > 0$) are less than 0.01.

		O(1)	O(2)	O(3)	C(1)	H(1)	H(2) = H(3)*
χ†		0.99	0.99	0.99	0.98	0.96	1.04
χ'		0.85	0.84	0.89	0.98	1.00	1.00
l	m						
0	0	6.22	6.15	6.36	4.20	0.65	0.71
1	1	−0.06	−0.08	−0.05	0.08		
1	−1	−0.04	−0.01	−0.00	0.01		
1	0					0.04	0.08
2	0	0.00	−0.09	−0.05	−0.24	0.05	0.05
2	2	−0.05	−0.03	−0.06	0.09		
2	−2	0.04	0.03	0.00	−0.03		
3	1	−0.03	−0.01	0.07	0.00		
3	−1	−0.02	−0.01	0.02	−0.03		
3	3	0.09	0.05	0.00	0.32		
3	−3	0.00		0.03	−0.05		
4	0	0.02	0.00	0.00	0.06		
4	2	0.01	0.03	0.00	0.04		
4	−2	0.02	−0.01	0.03	0.01		
4	4	0.01	0.03	−0.01	−0.04		
4	−4	0.02	0.01	0.00	−0.03		

* The water hydrogens were constrained to have the same valence density.

† χ and χ' are the radial screening constants for HF and Slater-type orbitals, respectively.

The map obtained reproduces the features published previously. Well pronounced bond maxima appear with peak heights of 0.55, 0.45 and 0.25 e Å^{-3} for the C—C, C=O and C—OH bonds, respectively.

These values fit in well with the trend established by Stevens & Coppens (1980) for bond peak heights as a function of resolution limit. The C—C bond density exhibits considerable π character as judged by its elongation perpendicular to the molecular plane, which has also been reported previously.

In the lone-pair region of the O(2) atom two distinct lobes, with slightly different peak heights are revealed. Their appearance is not as pronounced as would be expected for an sp^2 oxygen which can partly be explained by the restrictions applied to the data during summation.

$X - X$(mul) maps were also evaluated. The positional and thermal parameters obtained by multipole refinement were used to generate structure factors based on spherical atoms. Maps are displayed in Fig. 2(*a*), where a $\sin\theta/\lambda$ limit of 0.71 Å^{-1} was applied, and in Fig. 2(*b*) with all data being used. Here noticable changes in the heights of the bond and lone-pair densities are observed as compared with the map discussed above. The bond peaks are elongated and more excess density is shown in the non-bonding region of the O(2) atom. Charge depletion midway between the donor and acceptor atoms of

hydrogen bonds has been observed many times (Feil, 1988), and is attributed to the electrostatic nature of the interaction. These charge-deficient areas are well reproduced indicating that the thermal parameters of the H atoms are estimated properly. The inclusion of high-order data in the summation significantly emphasizes the peaks without dramatically increasing the noise level.

Fig. 2(*c*) shows the static model deformation density which might be compared directly with theoretical calculations. The residual map (Fig. 2*d*) $X - X$(mul) displays no significant features.

Acetamide

Experimental

Commercial acetamide crystals were found to be of sufficient quality for X-ray data collection. A well-formed hexagonal prismatic specimen (0.5 × 0.5 × 0.6 mm) was chosen and prepared on a Be needle as described previously. The crystal was mounted with the *c* axis only a few degrees from the φ rotation axis. At room temperature 1188 reflections were collected in the range $5 \le 2\theta \le 56°$. Conventional refinement [initial positional and thermal parameters from Denne & Small (1971)] with 415 independent reflections in space group *R*3*c* led to $R = 0.031$ and $wR = 0.029$ indicating good crystal quality.

The crystal was cooled down maintaining a temperature decrease of 0.6° min^{-1}. At seven temperatures between 300 and 20 K the crystal position and oricntation as well as the lattice parameters were redetermined by centering 50 reflections. Three reflections were monitored by means of $\omega/2\theta$ and φ scans within 20 K intervals in order to detect possible crystal defects during cooling. Lattice constants compared with those at 300 K are given in Table 5.

The temperature was fixed at 23 ± 1 K for data collection to allow later combination with the neutron data measured by Jeffrey *et al.* (1980) at that temperature. Data collection was carried out in the same region as before (5–56° in 2θ) and gave 1372 observations including intensity profiles with zero unobserved (there were ten at room temperature). Three reflections (300/030/125) were selected as standards and measured every hour. They were constant to within 1% during the entire measurement. After merging the symmetry-equivalent reflections an internal *R* value of 0.009 was obtained. Preliminary refinement using all observed data gave $R = 0.024$ and $wR = 0.023$ which made it worthwhile to collect data up to $2\theta = 104°$. In order to obtain the path length so as to treat for extinction, an absorption correction was applied. In just the same way a complete data set was measured at 100 K to compare the EDD maps at these two temperatures.

As the crystal remained stable for more than four weeks under the experimental conditions given, we carried out data collection at three additional temperatures, 12, 50 and 250 K, in the low-order region $5 \le 2\theta \le 56°$. Comparison of the X-ray intensity data at various temperatures shows that there is an enormous increase in intensity, especially for high-order reflections, when the sample temperature is reduced from 100 to about 20 K. This is illustrated for the (*h*00) reflection series in Fig. 3, where the relative intensity increase with respect to room temperature is given. It can be seen that up to medium diffraction angles (see, for example, the 12,0,0 reflection at $2\theta \simeq 50°$), the intensity difference between 100 and 20 K is only a few percent; however, for the 21,0,0 reflection at $2\theta \simeq 100°$, a factor of about 30 is seen between room temperature and 100 K. This factor increases to 120 for 20 K, so the intensity at 20 K is four times stronger than that at 100 K.

A more general assessment of the advantage of using 23 K data is shown in Fig. 4. Here, the quantity $I/\sigma(I)$ is plotted *versus* $\sin\theta/\lambda$ for 100 and 23 K. Each $I/\sigma(I)$ value is averaged for $\sin\theta/\lambda$ intervals of decreasing lengths so as to obtain roughly the same number of reflections per interval. Comparison of the two curves shows that at medium $\sin\theta/\lambda$, say 0.66 Å^{-1}, $I/\sigma(I)$ is greater, by a factor of 1.4, for 23 K compared to 100 K, whereas this factor increases to over 3.0 at the high-order limit of 1.08 Å^{-1}. It can be seen therefore, that temperature reduction to such extreme values as 20 K leads to a significant signal to background improvement with increasing scattering angle.

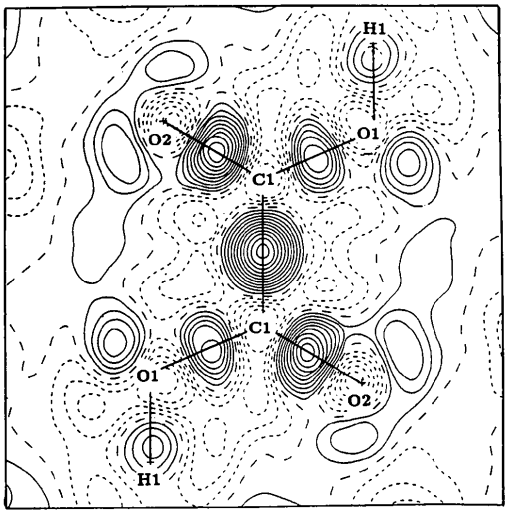

Fig. 1. $X_{low} - X_{high}$ electron deformation density (EDD) at 15 K of oxalic acid in the molecular plane. Contours are at 0.05 e Å^{-3}. Zero and negative lines dashed ($\sin\theta/\lambda \le 0.71$ Å^{-1}).

Structure refinement

(*a*) *Conventional refinement.* Full-order refinement was carried out on the 23 K data set using the positional parameters derived from neutron data (Jeffrey *et al.*, 1980) for all atoms and an estimated average isotropic displacement parameter. After a few cycles using first isotropic and later anisotropic displacement parameters for non-H atoms, an isotropic extinction parameter was refined and an R value of 0.026 was obtained. As expected, large H-atom shifts were found compared with the neutron results due to the aspherical distribution of electron density in the C—H and N—H bonds. Hereafter, the H-atom parameters were taken from neutron results, however, their anisotropic thermal parameters were scaled to the average value found in the X-ray refinement. Later, the H atoms were not refined. The isotropic extinction parameter dropped from 14.7 (1) to 1.12 (3) on decreasing the temperature from 295 to 23 K which must be due to an increase in the mosaic spread. Table 6 lists the atomic parameters at 100 and 23 K together with those from the multipole refinement at 23 K for comparison.

(*b*) *Multipole refinement.* For details of the refinement we refer to the corresponding section on oxalic acid. In the given local coordinate system (Fig.

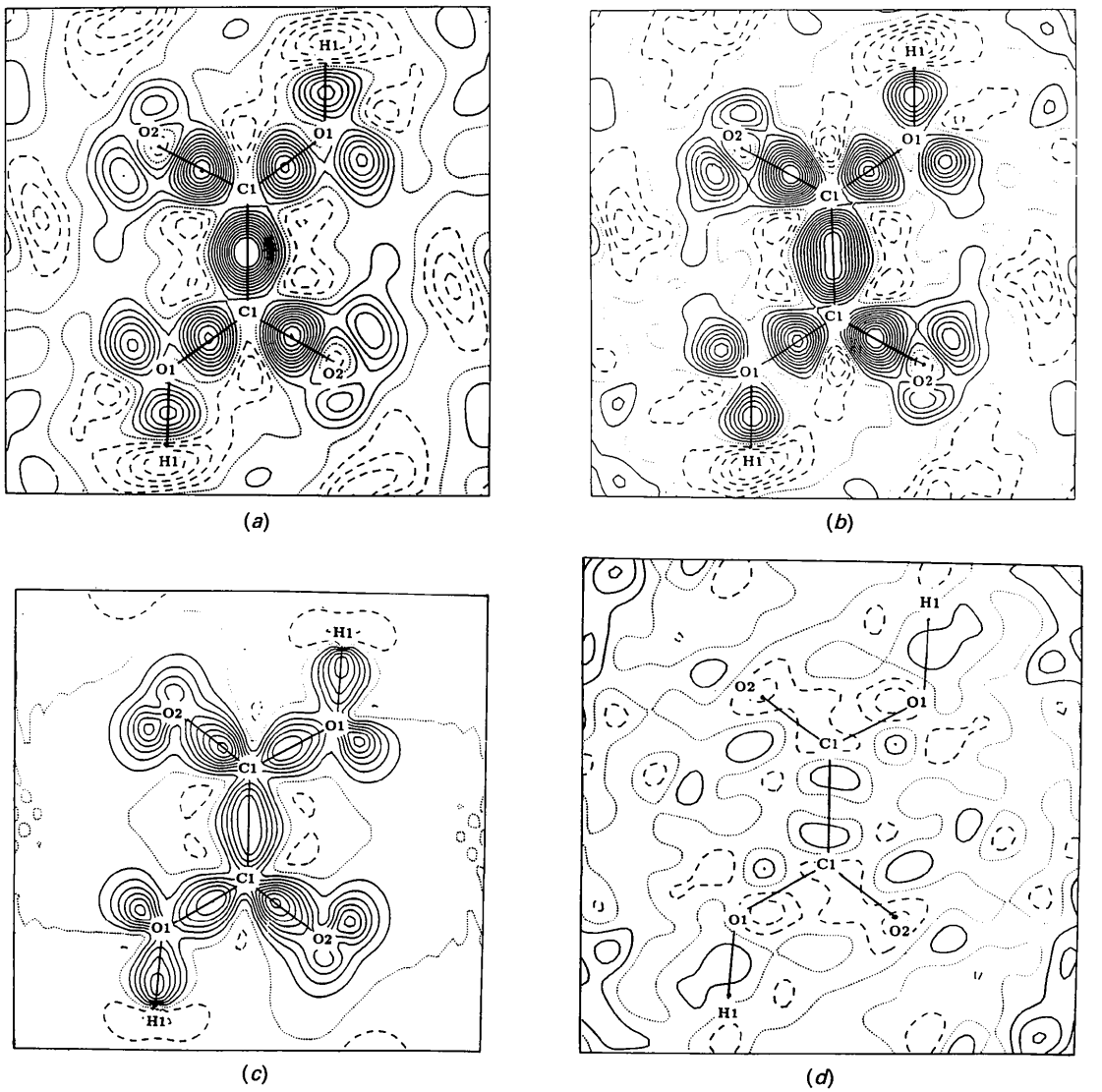

Fig. 2. Results of multiple treatment of oxalic acid at 15 K. Contours at 0.05 e Å^{-3}; zero level dotted, negative contours dashed lines, all in the molecular plane. (*a*) Dynamic map ($F_o - F_c^{sph}$) ($\sin\theta/\lambda \leq 0.71$ Å^{-1}). (*b*) Dynamic map ($F_o - F_c^{sph}$) ($\sin\theta/\lambda \leq 1.08$ Å^{-1}). (*c*) Static map. (*d*) Residual density map of (*c*).

Table 5. *Crystallographic and least-squares refinement data for acetamide at* 23 K *in comparison to room-temperature results*

Space group: $R3c$, $Z = 18$, $F(000) = 576$, $M_r = 59.07$, λ(Mo $K\alpha$) = 0.71069 Å (Nb filtered).

	Room temperature	100 K	23 K		
a (Å)	11.493 (2)	11.490 (2)	11.492 (2)		
c (Å)	13.547 (2)	13.045 (2)	12.892 (2)		
V (Å^3)	1549.02	1491.47	1474.75		
D_x (g cm^{-3})	1.140	1.184	1.197		
μ (cm^{-1})	0.98	1.02	1.03		
		Full order	High order	Full order	High order*
2θ (°)	5–56	5–104	56–104	5–104	56–104
$\sin\theta/\lambda$ (Å^{-1})	0.088–0.66	0.08–1.08	0.66–1.08	0.08–1.08	0.66–1.08
$N_{measured}$	1188	3819		3772	
N_{unique}	415	1739	1254	1729	1308
Unobserved $[F_o < 2\sigma(F_o)]$	10	82	81	17	17
NV	57	57	36	57	36
R_{int} (%)	1.60	1.75		1.29	
R (%)	3.11	4.20	4.95	3.02	2.73
wR (%)	2.94	3.81	4.88	3.08	2.04
Goodness of fit	3.81	2.78	1.97	2.56	1.24

Multipole refinement

N_{ref}	1684
NV	84
R (%)	2.16
wR (%)	1.89
Goodness of fit	1.61

* High-order X-ray, H atoms from 23 K neutron data.

8) the atomic site symmetries were assumed to be $mm2$ for N(1) and O(1), $3m$ for C(1) and m for C(2). In order to describe the valence deformation of the H atoms bond-directed dipoles were used and the conventional parameters were taken from the neutron measurement results. The multipole populations of the hydrogens in the NH_2 group were constrained to be equivalent.

Results from different least-squares refinements are summarized in Table 5.* Positional and displacement parameters (U_{ij}) are given in Table 6, the multipole population parameters are summarized in Table 7. Bond lengths and angles as well as hydrogen-bonded distances are shown in Table 8.

Deformation density

In order to calculate the deformation electron density maps, different cut-off values ($0.5 \leq \sin\theta/\lambda \leq 0.86$ Å^{-1}) were used to separate low- and high-order data. A value of $\sin\theta/\lambda = 0.66$ Å^{-1} turned out to deliver the best results in this case as judged by the resolution of the lone-pair region.

Electron deformation density in the plane of the molecule is given in Fig. 5(*a*). The H atoms were treated as described above. With the 100 K data the same procedures as described previously were carried out. The resulting EDD map is shown in Fig. 5(*b*). Experimental EDD maps were also generated using all data ($\sin\theta/\lambda \leq 1.08$ Å^{-1}) for both the 23 and 100 K data (Figs. 6*a* and 6*b* respectively). It can be seen that the increase in background noise is much more pronounced for the 100 K data, and in addition quite a few extra maxima showing both electron excess and holes are observed.

* A list of observed and calculated structure factors has been deposited with the British Library Document Supply Centre as Supplementary Publication No. SUP 55296 (34 pp.). Copies may be obtained through The Technical Editor, International Union of Crystallography, 5 Abbey Square, Chester CH1 2HU, England.

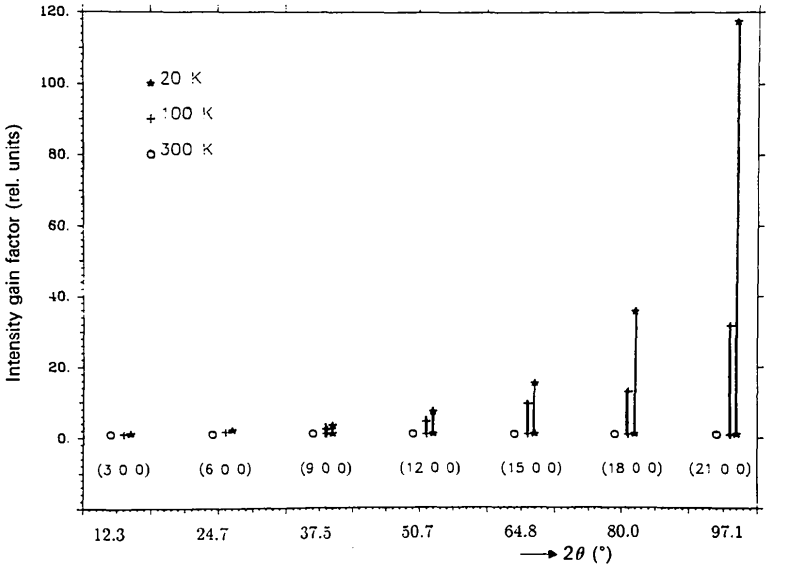

Fig. 3. Relative intensity gain factor for reflections of the (h00) series upon decreasing temperature for acetamide (each normalized to 300 K value).

Table 6. *Atomic parameters and displacement factors for acetamide at* 23 *and* 100 K, *with e.s.d.'s in parentheses*

FO = full-order data: $0.08 \le \sin\theta/\lambda \le 1.08$ Å^{-1}, HO = high-order data: $0.66 \le \sin\theta/\lambda \le 1.08$ Å^{-1}, ML = results of multipole refinement. H-atom values for HO and ML are from the neutron results (see text). Displacement factors of the form $T(\text{aniso}) = \exp\{-2\pi^2[U_{11}(ha^*)^2 + U_{22}(kb^*)^2 + U_{33}(lc^*)^2 + 2U_{12}hka^*b^* + 2U_{13}hla^*c^* + 2U_{23}kla^*b^*]\}$, $T(\text{iso}) = \exp[-2U(2\pi\sin\theta/\lambda)^2]$, with U_{ij} and U in Å^2 × 100.

(*a*) 23 K data

		x	*y*	*z*	U_{11}/U	U_{22}	U_{33}	U_{12}	U_{13}	U_{23}
C(1)	FO	0.47637 (5)	0.12947 (5)	0.03599 (–)	1.08 (2)	1.10 (2)	1.61 (2)	0.25 (1)	0.00 (1)	0.02 (2)
	HO	0.47626 (3)	0.12941 (3)	0.03599 (–)	1.066 (9)	1.095 (9)	1.53 (1)	0.226 (7)	−0.010 (7)	0.024 (8)
	ML	0.47619 (3)	0.12931 (3)	0.03540 (–)	1.04 (1)	1.08 (1)	1.52 (1)	0.23 (1)	−0.02 (1)	0.03 (1)
C(2)	FO	0.34060 (4)	0.00333 (5)	0.04012 (7)	0.90 (1)	0.95 (1)	1.13 (1)	0.39 (1)	−0.01 (1)	−0.07 (1)
	HO	0.34068 (3)	0.00341 (3)	0.04006 (4)	0.875 (8)	0.911 (8)	1.146 (7)	0.381 (6)	−0.037 (7)	−0.049 (7)
	ML	0.34072 (3)	0.00346 (3)	0.03947 (4)	0.822 (1)	0.881 (1)	1.14 (1)	0.34 (1)	−0.06 (1)	−0.05 (1)
O(1)	FO	0.24071 (4)	−0.00118 (5)	−0.00169 (6)	1.09 (1)	1.09 (1)	1.89 (2)	0.52 (1)	−0.23 (1)	0.06 (1)
	HO	0.24072 (3)	−0.00123 (3)	−0.00179 (4)	1.066 (8)	1.070 (8)	1.869 (9)	0.517 (6)	−0.258 (6)	0.073 (6)
	ML	0.24073 (4)	−0.00124 (3)	−0.00200 (2)	1.00 (1)	1.01 (1)	1.82 (2)	0.47 (1)	−0.24 (1)	0.09 (1)
N(1)	FO	0.33363 (5)	−0.10014 (5)	0.09152 (6)	1.07 (1)	1.07 (1)	1.60 (2)	0.43 (1)	−0.09 (1)	0.21 (1)
	HO	0.33361 (3)	−0.10027 (3)	0.09142 (3)	1.045 (8)	1.065 (8)	1.594 (9)	0.442 (7)	−0.105 (6)	0.198 (6)
	ML	0.33358 (3)	−0.10030 (3)	0.09100 (3)	0.99 (1)	1.02 (1)	1.56 (1)	0.42 (1)	−0.11 (1)	0.20 (1)
H(1)	FO	0.252 (2)	−0.175 (1)	0.106 (1)	3.5 (4)					
H(2)	FO	0.405 (1)	−0.099 (1)	0.1190 (9)	1.3 (2)					
H(3)	FO	0.482 (1)	0.180 (1)	0.097 (1)	2.8 (3)					
H(4)	FO	0.544 (2)	0.105 (2)	0.034 (1)	4.6 (4)					
H(5)	FO	0.483 (1)	0.192 (1)	−0.0196 (9)	2.9 (3)					

(*b*) X-ray full-order data at 100 K

	x	*y*	*z*	U_{11}/U	U_{22}	U_{33}	U_{12}	U_{13}	U_{23}
C(1)	0.47588 (8)	0.12817 (8)	0.03599 (–)	1.85 (3)	1.85 (3)	2.61 (3)	0.31 (2)	−0.07 (3)	0.11 (3)
C(2)	0.34017 (6)	0.00250 (7)	0.0408 (1)	1.56 (3)	1.56 (2)	1.99 (2)	0.65 (2)	0.03 (2)	−0.11 (2)
O(1)	0.24051 (6)	−0.00235 (7)	−0.00086 (9)	1.83 (2)	1.75 (2)	3.25 (3)	0.81 (2)	−0.37 (2)	0.14 (2)
N(1)	0.33303 (8)	−0.10035 (7)	0.09222 (9)	1.70 (2)	1.86 (3)	2.64 (3)	0.71 (2)	−0.20 (2)	0.34 (2)
H(1)	0.256 (2)	−0.168 (2)	0.099 (1)	5.5 (5)					
H(2)	0.399 (1)	−0.097 (1)	0.118 (1)	2.0 (3)					
H(3)	0.489 (2)	0.171 (2)	0.098 (1)	5.0 (5)					
H(4)	0.541 (2)	0.103 (2)	0.039 (1)	5.7 (5)					
H(5)	0.494 (2)	0.188 (2)	−0.027 (2)	6.7 (6)					

The experimental electron density map (Fig. 5*a*) shows clearly the expected strong maxima (between 0.4 and 0.5 e Å^{-3}) in the middle of the covalent bonds and two well resolved maxima in the lone-pair region (0.25 and 0.2 e Å^{-3}). Density maps perpendicular to the centres of the three non-hydrogen bonds are similar to those reported by Ottersen *et al.* (1980), but much more pronounced.

The electron holes located on the hydrogen-bond vectors are in accordance with those calculated by

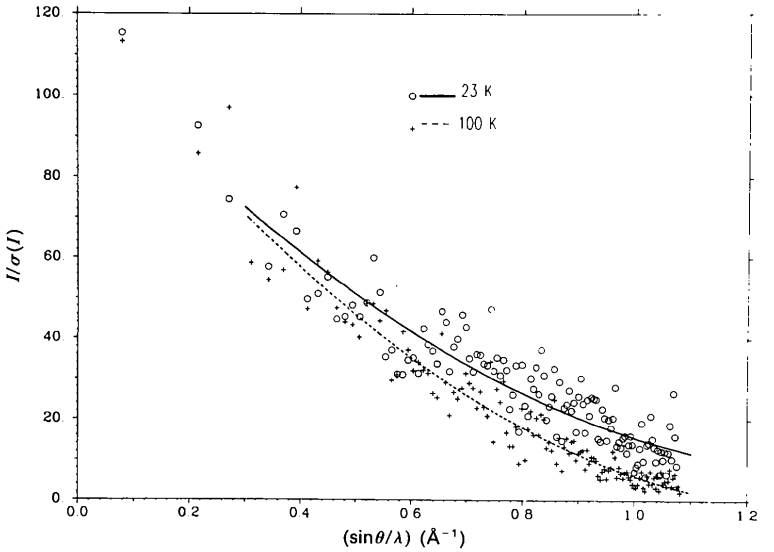

Fig. 4. $I/\sigma(I)$ plotted *versus* $\sin\theta/\lambda$ for the acetamide reflections at 23 K and at 100 K demonstrating the signal to background improvement especially for high-order data at 23 K. A least-squares second-order curve (Rudert, 1992) was used to approximate the contributing data.

Table 7. *Multipole refinement population parameters for acetamide at* 23 K

The other e.s.d.'s are the same as for oxalic acid dihydrate. For definition of χ see Table 4.

		O(1)	C(1)	C(2)	N(1)	H(1)	H(3)
χ		0.99 (1)	0.97 (1)	0.98 (1)	0.99 (1)	1.0 (–)	1.0 (–)
l	m						
0	0	6.18 (5)	4.31 (9)	4.19 (7)	5.25 (7)	0.89 (2)	0.77 (2)
1	1			0.01			
1	−1			0.07			
1	0	−0.01	−0.03		0.02	0.20	0.024
2	0	−0.02	−0.07	−0.22	0.02		
2	2	−0.08		0.04	−0.02		
2	−2			0.01			
3	0	0.03	0.32		0.15		
3	1			−0.06			
3	−1			0.08			
3	2	0.03			0.15		
3	3		0.02	0.26			
3	−3			0.06			
4	0	0.01	−0.06	−0.01	0.09		
4	2	0.02		0.04	−0.08		
4	−2			−0.04			
4	3		−0.05				
4	4	0.00		−0.03	0.02		
4	−4			−0.08			

Table 8. *Experimental bond lengths* (Å) *and angles* (°) *for acetamide, with e.s.d.'s in parentheses*

	23 K		100 K
	X-ray full data	High order*	Full data
C(1)—C(2)	1.5090 (6)	1.5071 (4)	1.5063 (9)
C(2)—O(1)	1.2456 (9)	1.2459 (6)	1.244 (1)
C(2)—N(1)	1.3284 (9)	1.3297 (6)	1.325 (1)
C(1)—H(3)	0.95 (2)		0.91 (2)
C(1)—H(4)	0.95 (2)		0.93 (3)
C(1)—H(5)	0.99 (1)		1.03 (2)
N(1)—H(1)	0.92 (1)		0.84 (2)
N(1)—H(2)	0.89 (1)		0.81 (2)
C(2)—C(1)—H(3)	106.0 (7)	108.50 (3)	107 (1)
C(2)—C(1)—H(4)	109 (1)	112.40 (3)	108 (1)
C(2)—C(1)—H(5)	112.7 (7)	111.20 (3)	116 (1)
H(3)—C(1)—H(4)	112 (1)	107.40 (2)	101 (2)
H(3)—C(1)—H(5)	102 (1)	106.90 (3)	115 (2)
H(4)—C(1)—H(5)	115 (1)	110.10 (2)	109 (2)
C(1)—C(2)—O(1)	120.90 (6)	120.90 (4)	120.9 (9)
C(1)—C(2)—N(1)	116.60 (5)	116.70 (3)	116.7 (8)
O(1)—C(2)—N(1)	122.50 (4)	122.40 (3)	122.4 (7)
C(2)—N(1)—H(1)	121 (1)	120.20 (4)	117 (2)
C(2)—N(1)—H(2)	122.8 (7)	120.00 (3)	122 (1)
H(1)—N(1)—H(2)	116 (1)	119.40 (4)	122 (1)

* High-order X-ray, $\sin\theta/\lambda(\text{min}) = 0.66$ Å^{-1}. H atoms from 23 K neutron data (Jeffrey *et al.*, 1980).

Mensching, von Nissen, Valtazanos, Ruedenberg & Schwarz (1988) for small molecules. The results of the EDD calculation for the 100 K data set (Fig. 5*b*) show a clearly reduced resolution in the region of the lone-pair electrons of O(1). Although the peak heights in most of the covalent bonds are approximately the same, more overlap is seen due to the stronger thermal smearing of the single atoms.

Ab initio calculations were carried out at the Hartree–Fock level using a 6-31G* basis set, with *d*-type polarization functions on non-H atoms (*GAUSSIAN*86; Frisch *et al.*, 1984). In order to simulate the intermolecular interactions caused by the hydrogen bonds four water molecules were placed in positions such that their H and O atoms coincided with the hydrogen-bonded atoms of the neighbouring acetamide molecules. A plot of the EDD in the molecular plane is shown in Fig. 7.

This map shows maxima which are in good agreement with the experimental map, at least as far as peak shape and position are concerned, and coincides quite well with the multipole static map of Fig. 8.

Results and discussion

Lattice parameters (normalized to 300 K values) *versus* temperature are plotted in Fig. 9(*a*). It can be seen that the *a* axis does not change at all with temperature, whereas the *c* axis decreases by approximately 5%. This can probably be attributed

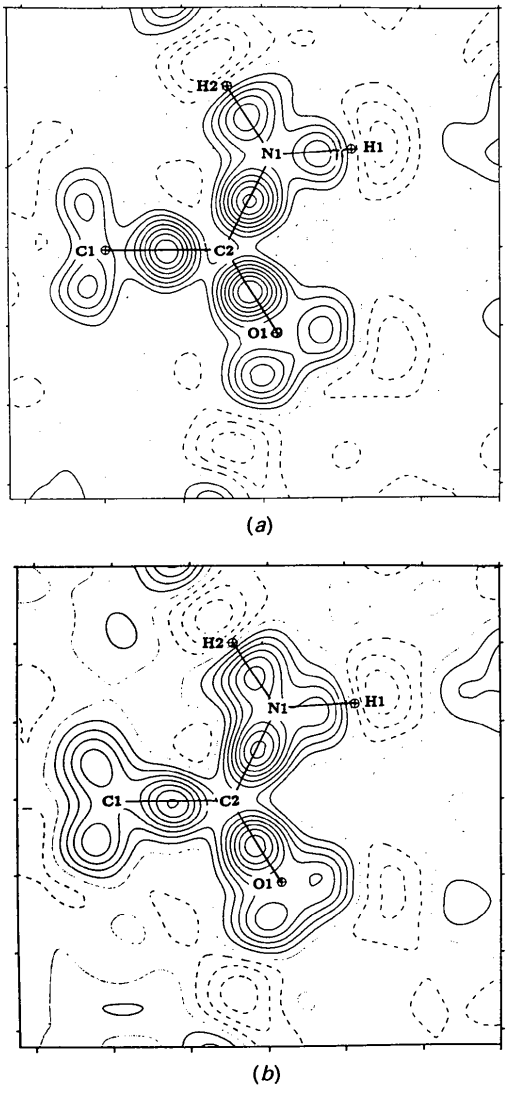

Fig. 5. $X_{low} - X_{high}$ electron deformation density (EDD) map of acetamide. Contours at 0.05 e Å^{-3}, zero and negative lines dashed: $\sin\theta/\lambda \le 0.66$ Å^{-1}. (*a*) At 23 K. (*b*) At 100 K.

to the weak intermolecular interactions in this direction, which are much stronger in the *ab* plane, where the four hydrogen bonds have their main vector components.

Bond lengths and angles (Table 8) agree very well with those from neutron diffraction (Jeffrey *et al.*, 1980), except for the H atoms, for which the bond distances are 0.1 to 0.2 Å shorter than those from the neutron data, as expected for X-ray measurements. In the case of the molecular geometry, *e.g.* planarity of the non-H atoms, the conformations of the amide and methyl groups are essentially the same (within 3σ) as reported by Jeffrey (1980) and are not discussed in detail here.

Since at least low-order data were available at six different temperatures (12, 23, 50, 100, 250 and 300 K), anisotropic displacement parameters based on low-order refinement could be compared for these temperatures. Fig. 9(*b*) gives an impression of their decreasing values at low temperature, displaying the principal-axes components of O(1) and C(1) *versus* *T*. The average reduction in U_{ii} values from room temperature to 12 K is by a factor of approximately 4; to 100 K this factor is 2.5. It follows that reduction of the temperature from 100 to 12 K leads to an average decrease in the U_{ii} values of about 33%.

Comparison of the 23 K displacement parameters for different refinements based on X-ray data with

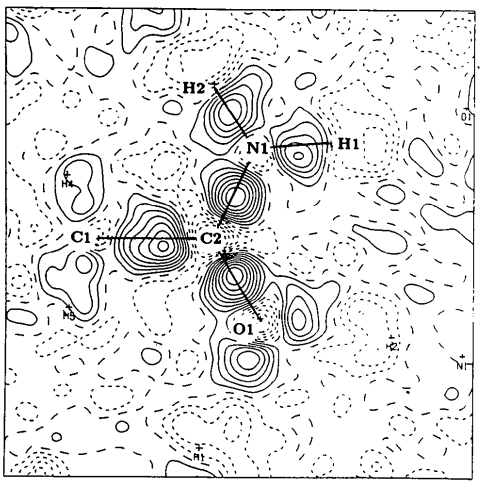

(*a*)

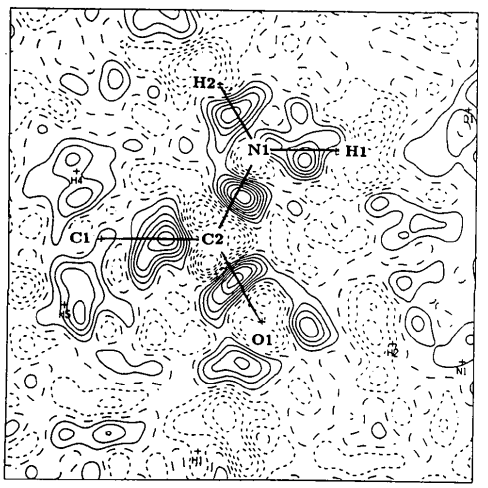

(*b*)

Fig. 6. Same as Fig. 5 but $\sin\theta/\lambda \leq 1.08$ Å^{-1}. (*a*) At 23 K. (*b*) At 100 K.

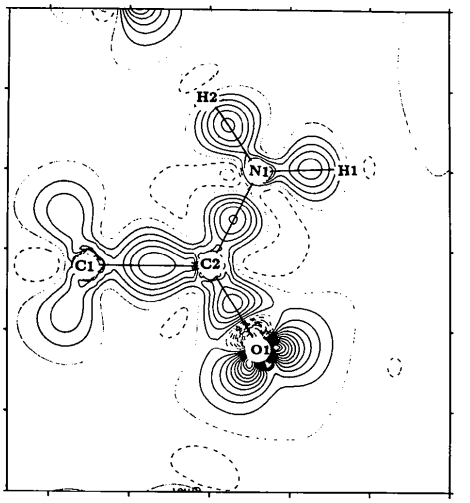

Fig. 7. Theoretical deformation density for acetamide. Contours at 0.1 e Å^{-3}, zero level is dotted, negative contours dashed.

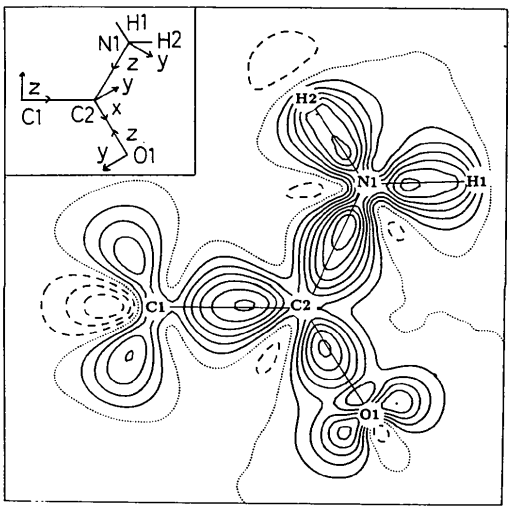

Fig. 8. Multipole static map of acetamide at 23 K. Contours at 0.1 e Å^{-3}. Local coordinate system used is shown in the upper-left corner.

the corresponding neutron data is made in Table 9. Firstly, it can be seen that the differences between full- (FO) and high-order (HO) refinement are rather small, but amount to almost 10%, if full-order and multipole refinement data are compared [see for example, U_{11} for C(2)]. Secondly, the ratios between X-ray and neutron data are different in that X-ray values are more than 50% higher. Moreover, the ratios are different for different atoms and also between the three principal axes. This explains why an overall scaling of the neutron displacement parameters in the course of $X-N$ map generation led to unsatisfactory results. The EDD maps obtained showed huge holes at certain atomic sites and were also poor in quality when compared to all maps for which non-H-atom parameters were generated from X-ray data alone.

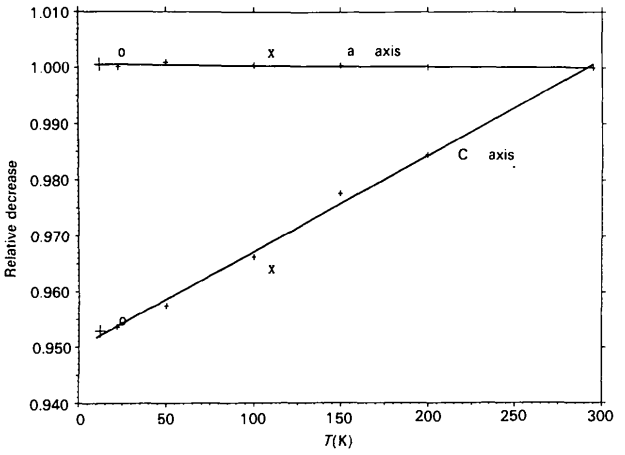

(*a*)

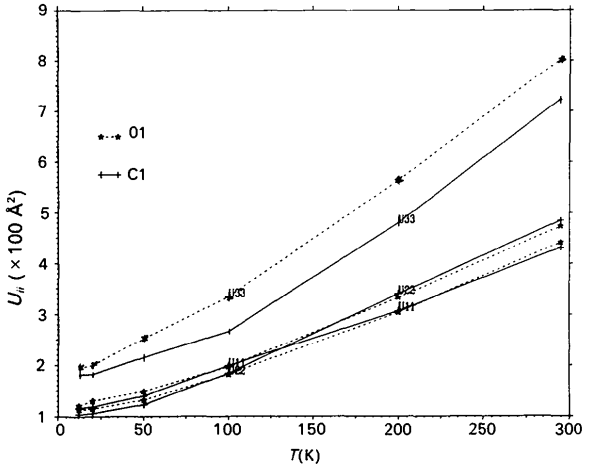

(*b*)

Fig. 9. (*a*) Cell and (*b*) displacement parameter dependence upon decreasing temperature for acetamide. In (*a*), +, × and o refer to this work, Ottersen (1975) and Jeffrey *et al.* (1980), respectively.

Table 9. *Ratio of U_{11}, U_{22} and U_{33} displacement parameters for full (FO), high-order (HO) and multipole refinement (ML) in relation to the neutron data*

	U_{11}	U_{22}	U_{33}	
C(1) FO	1.66	1.62	1.59	
HO	1.64	1.66	1.51	
ML	1.60	1.63	1.50	$av_{C(1)}$ = 1.58 (7)*
C(2) FO	2.0	2.02	1.69	
HO	1.94	1.94	1.71	
ML	1.82	1.86	1.70	$av_{C(2)}$ = 1.79 (8)*
O(1) FO	1.91	1.76	1.69	
HO	1.87	1.73	1.67	
ML	1.76	1.62	1.63	$av_{O(1)}$ = 1.67 (8)*
N(1) FO	1.53	1.51	1.51	
HO	1.49	1.50	1.50	
ML	1.41	1.44	1.47	$av_{N(1)}$ = 1.44 (3)*
	$av_{U_{11}}$ = 1.65 (18)*	$av_{U_{22}}$ = 1.64 (17)*	$av_{U_{33}}$ = 1.58 (11)*	

$Average_{total}$ = 1.62 (15)*

*Averages calculated from the multipole refinement data (ML) only.

Results of thermal-motion correction for the three temperatures, 23, 100 and 300 K (Schomaker & Trueblood, 1968), are summarized in Table 10. The corrected non-H bond lengths at 23 K are given in Table 10 and compared with those obtained at 100 and 300 K.

In order to check the quality of the density maps generated without the use of any neutron data, even for the hydrogens, we calculated positional hydrogen parameters by shifting the H atoms along the X-ray C—H and N—H bond vectors to distances of 1.08, and 1.02 Å respectively, assuming that the directions of the corresponding hydrogen bonds are essentially correct. This assumption is justified since the angles between the X-ray and neutron vectors were found to be less than 5°. A density map obtained in such a way and using isotropic displacements for the hydrogens showed no significant differences compared to the map obtained with H-atom parameters from neutron scattering.

Concluding remarks

Our first low-temperature experiments with the diffractometer described in this paper show that the instrument delivers high-quality data suitable for accurate structure and charge-density determination.

The experimental electron density of oxalic acid, as compared with numerous studies at 100 K, shows improved resolution that could be attributed to the increased accuracy, especially of the high-order data. Thus the standard parameters obtained from the high-order refinement are expected to be less biased than those introduced by the spherical-scattering model. Inclusion of the high-order reflections in the Fourier calculation enhanced the bond and lone-pair peaks in the dynamic deformation density maps without decreasing the signal to noise ratio.

Table 10. *Bond lengths* (Å) *resulting from rigid-body thermal-motion analysis*

	23 K		23 K*		100 K		300 K	
	Obs	Corr	Obs	Corr	Obs	Corr	Obs	Corr
C(1)—C(2)	1.5091 (7)	1.513	1.5094 (10)	1.513	1.507 (1)	1.520	1.505 (2)	1.519
C(2)—O(1)	1.245 (1)	1.252	1.2468 (12)	1.250	1.244 (2)	1.250	1.226 (2)	1.233
C(2)—N(1)	1.330 (1)	1.335	1.3351 (11)	1.337	1.330 (2)	1.336	1.324 (3)	1.333

*Jeffrey *et al.* (1980).

The advantages of low-temperature data collection are demonstrated by the study on acetamide where the relative intensities $[I(T)/I(300\ \mathrm{K})]$ at a given T (100, 20 K) are found to increase exponentially as a function of the scattering angle. A similar increase occurs for a given reflection when the temperature is lowered. This trend corresponds to the temperature dependence of the thermal parameters. For $T > 50$ K the mean-square displacements are essentially proportional to the temperature, while for $T < 50$ K they tend to be independent of the temperature. This variation is in good agreement with the prediction of an effective mean-field harmonic oscillator model.

The results presented here seem to show that, in spite of the considerable technical efforts, it is worthwhile collecting X-ray single-crystal data around 20 K.

This work was funded by the Deutsche Forschungsgemeinschaft (DFG). Funds are also acknowledged from the Fonds der Chemischen Industrie. Moreover, we thank Thomas Richter for the *ab initio* calculations on acetamide.

References

ALLIBON, J. R., FILHOL, A., LEHMANN, M. S., MASON, S. A. & SIMMS, P. (1981). *J. Appl. Cryst.* **14**, 326–328.
BECKER, P. & COPPENS, P. (1974). *Acta Cryst.* A**30**, 148–153.
COPPENS, P. (1984). *Acta Cryst.* A**40**, 184–195.
COPPENS, P. & LEHMANN, M. S. (1976). *Acta Cryst.* B**32**, 1777–1784.
DENNE, W. & SMALL, R. W. H. (1971). *Acta Cryst.* B**27**, 1094–1098.
FEIL, D. (1988). *Port. Phys.* **19**, 21–42.
FELD, R. & LEHMANN, M. S. (1979). Unpublished results.
FRISCH, M. J., BINKLEY, J. S., SCHLEGEL, H. B., RAGHAVACHARI, K., MELIUS, C. F., MARTIN, L., STEWART, J. J. P., BOBROWICZ, F. W., ROHLFING, C. M., KAHN, L. R., DEFREES, D. J., SEEGER, R., WHITESIDE, R. A., FOX, D. J., FLEUDER, E. M. & POPLE, J. A. (1984). *GAUSSIAN*86. Carnegie-Mellon Quantum Chemistry Publishing Unit, Pittsburgh, PA, USA.
GABE, E. J. (1981). Chemistry Division, NCR, Ottawa, Canada. Private communication.
HALL, S. R. & STEWART, J. M. (1987). Editors. *XTAL*2.2 *Users Manual.* Univs. of Western Australia, Australia, and Maryland, USA.
HAMILTON, W. C. (1965). *Acta Cryst.* **18**, 866–870.
HANSEN, N. K. & COPPENS, P. (1978). *Acta Cryst.* A**34**, 909–921.
HENDRIKSEN, K., LARSEN, F. K. & RASMUSSEN, S. E. (1986). *J. Appl. Cryst.* **19**, 350–354.
JEFFREY, G. A., RUBLE, J. R., MCMULLAN, R. K., DE FREES, D. J., BINKLEY, J. A. & POPLE, J. A. (1980). *Acta Cryst.* B**36**, 2292–2299.
JEFFREY, G. A., RUBLE, J. R. & YATES, J. H. (1983). *Acta Cryst.* B**39**, 388–394.
KING, H. E. & FINGER, L. W. (1979). *J. Appl. Cryst.* **12**, 374–378.
LANGE, J., BURZLAFF, H. & NEUGEBAUER, H. (1988). *Z. Kristallogr.* **185**, 674.
MENSCHING, L., VON NISSEN, W., VALTAZANOS, P., RUEDENBERG, K. & SCHWARZ, W. H. E. (1989). *J. Am. Chem. Soc.* **111**, 6933–6941.
OTTERSEN, T. (1975). *Acta Chem. Scand. Ser. A*, **29**, 939–944.
OTTERSEN, T., ALNLÖF, J. & HOPE, H. (1980). *Acta Cryst.* B**36**, 1147–1154.
RUDERT, R. (1992). Private communication.
SCHOMAKER, V. & TRUEBLOOD, K. N. (1968). *Acta Cryst.* **11**, 774–781.
STEVENS, E. D. & COPPENS, P. (1980). *Acta Cryst.* B**36**, 1864–1876.
WEBER, H. P., CRAVEN, B. M., SAWZIK, P. & MCMULLAN, R. K. (1991). *Acta Cryst.* B**47**, 116–117.
ZOBEL, D. & LUGER, P. (1990). *J. Appl. Cryst.* **23**, 175–179.